UNIVERSITÀ DI PARMA
ARCHIVIO DELLA RICERCA

University of Parma Research Repository

Phase-field slip-line theory of plasticity

This is a pre print version of the following article:

Original
Phase-field slip-line theory of plasticity / Freddi, Francesco; ROYER CARFAGNI, Gianni. - In: JOURNAL OF THE MECHANICS AND PHYSICS OF SOLIDS. - ISSN 0022-5096. - 94:(2016), pp. 257-272. [10.1016/j.jmps.2016.04.024]

Availability:
This version is available at: 11381/2812181 since: 2021-10-22T12:49:28Z

Publisher:
Elsevier Ltd

Published
DOI:10.1016/j.jmps.2016.04.024

Terms of use:

Anyone can freely access the full text of works made available as "Open Access". Works made available

Publisher copyright

note finali coverpage

(Article begins on next page)

02 May 2026

Phase-field slip-line theory of plasticity

Francesco Freddi[a], Gianni Royer-Carfagni[b,*]

[a] *Department of Civil-Environmental Engineering and Architecture, University of Parma, Parco Area delle Scienze 181/A, I 43124 Parma, Italy*

[b] *Department of Industrial Engineering, University of Parma, Parco Area delle Scienze 181/A, I 43124 Parma, Italy. Presently: Cullen College of Engineering, University of Houston, 4726 Calhoun Rd, Houston, TX 77204-4003, USA*

Abstract

A variational approach to determine the deformation of an ideally plastic substance is proposed by solving a sequence of energy minimization problems under proper conditions to account for the irreversible character of plasticity. The flow is driven by the local transformation of elastic strain energy into plastic work on slip surfaces, once that a certain energetic barrier for slip activation has been overcome. The distinction of the elastic strain energy into spherical and deviatoric parts is used to incorporate in the model the idea of von Mises plasticity and isochoric plastic strain. This is a "phase field model" because the matching condition at the slip interfaces are substituted by the evolution of an auxiliary phase field that, similarly to a damage field, is unitary on the elastic phase and null on the yielded phase. The slip lines thus diffuse in bands, whose width depends upon a material length-scale parameter.

Numerical experiments on representative problems in plane strain give solutions with striking similarities with the results from classical slip-line field theory, but the proposed model is much richer because, accounting for elastic deformations, it can describe the formation of slip bands at the local level, which can nucleate, propagate, widen and diffuse by varying the

*Corresponding Author. Tel.: +39 0521 906606; fax: +39 0521 905705

Email addresses: francesco.freddi@unipr.it (Francesco Freddi), gianni.royer@unipr.it (Gianni Royer-Carfagni)

boundary conditions. In particular, the solution for a long pipe under internal pressure is very different from the one obtainable from the classical macroscopic theory of plasticity. For this case, the location of the plastic bands may be an insight to explain the premature failures that are sometimes encountered during the manufacturing process. This practical example enhances the importance of this new theory based in the mathematical sciences.

Keywords: Phase field model, elasticity, plasticity, slip line field theory, slip bands, variational approach.

---

1. Introduction

The mathematical description of the plastic deformation of materials is traditionally obtained by assuming that the total strain in the body can be decomposed additively (or multiplicatively in the case of finite deformations) into two regular fields: the part that is due to the *reversible* elastic distortion of the constituent volume elements, and the part that is associated with the *non-reversible* modification of their shape. In the case of metals, the first comes from small variation of the interatomic distance, whereas the second one is produced by a re-arrangement of the crystalline lattice facilitated by dislocation glide. Yield criteria, flow rules and hardening laws allow to determine the deformation associated with the prescribed boundary conditions [1].

In the case of a perfectly-plastic substance, with no work hardening, the deformation can unboundedly grow when the yield limit is attained. The *plastic flow* is constrained by the applied boundary condition and the problem consists in finding the corresponding strain rate. In these situation, one can certainly neglect the elastic straining with respect to the plastic distortion, and model the material as rigid-plastic. Since the volume change is null, the problem can be solved in terms of the stress state only and associated yield function, usually derived either from the Tresca or von-Mises criterion. The plastic equation are hyperbolic, and the corresponding characteristics of shear-stress and shear-strain-velocities coincide. In plane strain conditions, the characteristics form two orthogonal families of curves, traditionally referred to as *slip lines*, whose direction coincide at every point with

the those of the maximum shear strain rate. Slip-line theory [2, 1], introduced by Prandtl, Hencky and Geiringer [3], aims at identifying the plastic state considering the field of slip lines as the fundamental unknown to be determined.

The theory of the surfaces of slip represents a mesoscopic interpretation of the phenomena occurring at the micro-level associated with strain localization such as in the case of the formation of Lüders bands. The singular character of the deformation is lost in the traditional mathematical theory of plasticity, which instead provides a smeared macroscopic view of plastic distortions through a regular macroscopic plastic-strain field. This represents an averaged description of a structured deformation [4], produced by the localization of plastic distortions in narrow slip (or glide) bands. Such a mechanisms characterizes the response of various substances over a broad range of scales, from several miles of the lithosphere [5], down to the nano-level of metallic glasses [6]. Localization in the form of shear bands usually represents the pre-failure deformation also of natural rocks [7], granular materials [8] and polymers [9].

In metallic alloys, plasticity is associated with microscopic glide along Lüders bands, which is justified at the atomic level by the movement of dislocations ([10] Sect. 13). Activation of gliding along such bands requires the overcoming an energetic barrier, which allows to maintain a pure elastic phase when the strain is relatively small, while the onset of the plastic phase is marked by a sharp well point. Such a barrier is associated with the anchoring of the dislocations in the energetic wells produced by the presence of solute atoms in the metallic lattice. Under moderate strain the dislocations remain anchored and deformation is purely elastic, but in overstrained condition, dislocations are unpinned and can glide to produce inelastic distortions. This mechanism can also give reasons for the transition from an upper to a lower yield point that is evident in the experiments, interpreted in [11] through a simple but effective mechanical model, consisting in a particular arrangement of spring-dashpot units.

Although dislocation movements should produce sliding at the atomic level, preferential paths along macroscopic glide layers, or super-bands, can be favored by other phenomena,

such as initial stress concentrations in the elastic regime. Nadai has provided an impressive set of beautiful pictures of the formation of such bands produced by notches and holes [2]. In polycrystal the phenomenon is usually triggered by nucleation of micro-holes from brittle micro-cracking or decohesion of inclusions [12]. As the strain is increased, the small voids coalescence through a band of localized shearing, whose progression presents strict similarities with a crack opening because it is associated with energy consumption. Plastic localization in super-bands has been observed in cylindrical bars under large torsional strains made of AISI 4340 steel [13] and mild carbon steel [14]. The onset of plastic deformation is marked by the formation of thin Lüders-like bands in the transversal direction but, as the twist is augmented, single coarse slip bands form in a longitudinal direction where shear deformation is concentrated, which progress and open like as a fracture in mode II as the strain is augmented [13]. Strain localization in super bands may also be facilitated by geometric effects (instabilities), as demonstrated in the famous experiments by Körber and Siebel [15] on wide flat bars obtained from thin metal sheets when tested in tension. Judged as three-dimensional cases, problems of this kind involve "geometric" as opposed to "material" instability, but when modeled as two-dimensional continua, the localization is equivalent to the post-critical phenomenon associated with the surmounting of an energetic barrier [16]. The progression of shear super-bands in a crack-like manner, rather than being the consequence of a sudden bifurcation from a uniform deformation field, has been confirmed in many experiments on metallic alloys [17].

The mathematical modelling of strain localization can follow two different approaches. It can be considered as an instability [18], predictable by the pre-localization constitutive relations of the material: at critical conditions a bifurcation occurs from a smoothly varying deformation into a highly concentrated shear band mode [19]. Otherwise, it can be inferred that alternative competing physical mechanisms of deformation come into play at a certain stage of the load history. The transition from one to the other should be triggered by an irreversible event with consequent energy dissipation, such as the rupture of an anchoring ligament. Assuming that an energetic barrier has to be overcome to unpin a slip surface is

mandatory, because no pre-localization (elastic) stage would be possible if this contribution goes to zero, otherwise the body would present no resistance against plastic gliding at any level of strain. This rationale has been assumed by Palmer and Rice [20] to model the growth of localized shear bands in the progressive failure of over-consolidated clay or sand, by introducing an energetic competition à la Griffith for the propagation of the tip of a concentrated shear band into the sound material.

If one accepts that the plastic deformation is due to strain localization along slip surfaces of infinitesimal thickness, the kinematical description of yielding presents strict similarities with mode II fracture, in the fact that it allows for discontinuities in the displacement fields along the gliding surfaces. However, whereas in classical brittle fracture the surface energy is either independent or a fast-decreasing function of the crack opening, the work to let the surfaces slip is never zero whatever the amount of slip is. Therefore, models of this kind can interpret the intermediate asymptotic stage of plastic flow, but not the phenomena that eventually lead to failure. A mathematical description of this type of plastic flow has been presented in [21] for the case of antiplane shear. Under the hypothesis that sliding occurs at constant shear stress (perfectly plastic body), the deformation consequent to an applied load history is found as the solution of a sequence of minimization problems for a functional of the displacement field, introducing an energetic competition between (reversible) elastic straining and (irreversible) plastic glide along unknown *free-discontinuity* slip surfaces. The minimization is sought under irreversibility conditions for the inelastic phenomena. A key hypothesis is consideration of a primitive energetic barrier for plastic slip analogous to fracture energy, i.e., an energy *per* unit area has to be expended right at the beginning to unpin any two gliding surfaces. Without such a contribution, a purely elastic phase could never be attained because plastic slip would occur just "touching" the body.

The model leads to a free-discontinuity variational problem set in the space of SBV functions that is difficult to handle. Remarkably, within the framework of $\Gamma-$convergence [22], it is shown in [21] that the energy functional can be approximated by a sequence of regularized

two-field elliptic functionals, where one field represents the macroscopic displacement in the body, while the second one denotes the local value of an order parameter, of the type commonly employed to describe phenomena of phase transition, which is 0 for the sound state of the body and 1 for the yielded state. The regularized theory fits in the class of phase-field models, for which the regularization is obtained through the introduction of gradient terms inducing a rapid, but smooth, transition on both sides of the interface *in lieu* of a sharp discontinuity. To this respect, the regularized variational model for plastic slip present similarities with the phase-field models of fracture [23], although it differs because of the addition of a surface energy term, accounting for the work to be consumed in plastic gliding. It also represents a particular two-dimensional extension of the general theory proposed in [24] for the one-dimensional case.

The numerical implementation of the regularized model, extended to the two-dimensional case of plane strain, has been conducted in [25]. Numerical experiments on paradigmatic case-studies have confirmed that the plastic strain concentrates in bands, but the bands may coalesce to form a plastic region, depending upon the shape and size of the body, the presence of pre-existing defects (voids, holes, notches) and the values of the governing parameters. Although results are in fair agreement with those obtained with the classical continuum plasticity theory, the model suffers some major drawbacks. First of all, the plastic bands are more similar to mode I cohesive fractures than to glides surfaces, because the bands in general form at right angle to the direction of maximal tensile stress and the plastic strain associated with them is coaxial with the stress. Moreover, since the model is defined by quadratic quantities it is symmetric in tension-compression, but this does not rule out the possibility of plastic contractions causing an unrealistic material interpenetration.

The purpose of this article is to conceive a plasticity theory based upon energy minimization by altering the associated functional to incorporate idea of "deviatoric-strain-driven" plastic slip, in agreement with the most traditional plasticity theories. The proposed model allows to calculate a slip-line framework of interface bands where shear-strain localizes, so to approximate the kinematics of the relative gliding of the neighboring surfaces, with no

risk of material interpenetration. The elasticity of the body is not neglected and, indeed, it represents an indispensable feature of the model, because the process is governed by an energetic competition between elastic deformation and plastic slip. The width of the slip bands depends upon a characteristic material parameter that also governs their relative spacing and, consequently, their number, but the slip-band pattern remains substantially unaltered. Numerical experiments on paradigmatic problems confirm that this approach is able to reproduce the slip-band pattern that can be inferred starting from the traditional theory, with a computational effort substantially moderate due to the fact that the deformation is described by smooth fields. We repute this approach much richer and more comprehensive than the traditional macroscopic theories of plasticity, since it provides indication on the mechanism of strain localization due to inelastic glide.

2. Phase field model for non-smooth plasticity

After revisiting various variational formulations that associate the plastic deformation with the formation of slip bands, we propose a new theory that represent the counterpart, for this type of problems, of a plasticity theory *à la* von Mises, driven by the deviatoric part of the strain energy.

2.1. Strong and weak formulations in antiplane shear

For the sake of completeness, it is useful to first recall the main results of the mathematical theory proposed in [21] for the case of antiplane shear. Suppose that $\Omega \subset \mathbb{R}^2$ represent the undistorted reference configuration of the cross section of a cylindrical body and let $u : \Omega \to \mathbb{R}$ indicate the corresponding out-of-plane displacement. The body is linear elastic with shear modulus μ, but plastic slip can localize on surfaces orthogonal to the plane of Ω, where the field u exhibits the jump $|u^+ - u^-|$ in absolute value. Let $S_u \in \Omega$ be the trace of all the discontinuity surfaces on Ω. From a mathematical point of view, the variational problem needs to be set in the space of Special functions of Bounded Variation $SBV : \Omega \to \mathbb{R}$, that

not only allows for discontinuities of u, but implies that the jump set S_u of u is rectifiable [26], i.e., in rough terms it is a curve contained in Ω.

One can then define the functional $\Pi(u)$ for the energy per unit-height of the body, as

$$\Pi(u) = \frac{\mu}{2}\int_{\Omega\setminus S_u} |\nabla u|^2 d\mathbf{x} + \gamma\,\mathrm{meas}(S_u) + \sigma_0 \int_{S_u} |u^+ - u^-|\, dr\,, \tag{2.1}$$

where σ_0 is the yielding stress, whereas γ represents an "activation" energy per unit area, analogous to Griffith's, that needs to be expended to nucleate new plastic slip. The strong formulation for the case of antiplane shear consists in the minimization problem

$$\min_{u\in\mathcal{A}} \Pi(u)\ ,\quad \mathcal{A} = \{u \in SBV(\Omega,\mathbb{R}) : u = \bar{u}\ \text{on}\ \partial\Omega^{\mathcal{D}}\}\,, \tag{2.2}$$

where $\partial\Omega^{\mathcal{D}}$ is that part of the boundary $\partial\Omega$ where Dirichlet boundary conditions $u = \bar{u}$ are assigned, whereas the remaining part, identified by $\partial\Omega^{\mathcal{N}} = \partial\Omega \setminus \partial\Omega^{\mathcal{D}}$, is supposed to be traction-free.

This approach establishes an energetic competition between three terms: *i*) the *elastic* strain energy, which provides the driving force; *ii*) the *surface activation* energy that is necessary to unpin the slip in the unitary area; *iii*) the work dissipated against the *cohesive* forces at yielding during the plastic glide. The plastic part of the deformation is associated with the discontinuities in the displacement field due to plastic slips and, to this respect, this approach presents analogies with that of cohesive fracture. It is worth remarking that, as discussed in [21], without the surface-activation term there would be no purely elastic phase, because plastic glide would spread at any whatever small level of strain[1]. Indeed, it is the presence of

[1]This conclusion is not valid in the 1-D case, for which the model of (2.1) and (2.2) results included, as a particular case, in the class of functionals considered in [27] for cohesive crack propagation in bars. It is shown in [27] that just a cohesive energy term à la Barenblatt (no activation term) is sufficient to account for a purely elastic phase at small strains. Evidently, the 1-D case cannot account for stress concentrations, that instead occur at the border of a slipping surface and are captured only by increasing the dimension

such term that introduces a yield limit in the material. For mild steel, it can be supposed to be representative of the energetic barrier that has to be overcome to unpin the dislocations and produce the orderly formation of shear bands [11]. For rocks and geomaterials, like over-consolidated clay or sand, it can model the work necessary to break the ligaments at the tip of a localized shear band before gliding can start [20].

The main results of [21] consists in demonstrating that the strong formulation can be approximated, in the sense of $\Gamma-$convergence, by a weak (regularized) formulation. To do so, define the auxiliary field $s : \Omega \to [0, 1]$, whose significance is analogous to that of a damage parameter since $s = 1$ where the material is sound and $s = 0$ where yielding has occurred. Both u and s are regular fields (*with no discontinuities*) belonging to the Sobolev space $W^{1,2}(\Omega, \mathbb{R})$ of functions with square-summable derivatives (in the sense of distributions). The *regularized* minimization problem is

$$\min_{u \in \hat{\mathcal{A}}} \Pi_l(u, s) \ , \quad \hat{\mathcal{A}} = \{(u, s) \in W^{1,2}(\Omega, \mathbb{R}) \times W^{1,2}(\Omega, \mathbb{R}) : u = \bar{u} \,\text{and}\, s = 1 \,\text{on}\, \partial\Omega^{\mathcal{D}}\} \,, \tag{2.3}$$

where the energy functional $\Pi_l(u, s)$ reads

$$\Pi_l(u, s) = \frac{\mu}{2} \int_\Omega (s^2 + o_l)|\nabla u|^2 d\mathbf{x} + \frac{\gamma}{2} \int_\Omega \left(l|\nabla s|^2 + \frac{(1-s)^2}{l} \right) d\mathbf{x} + \sigma_0 \int_\Omega (1-s)^2 |\nabla u| d\mathbf{x} \,. \tag{2.4}$$

The quantity o_l, usually supposed to be very small, is introduced to stabilize the regularized formulation.

The parameter s evolves according to an energetic competition stated by the minimization problem (2.3). Observing the expression (2.4), in order to minimize the elastic part of the energy s should be zero, but this produces, on the other hand, the increase of the term

of the space where the problem is set. Such stress concentrations cannot be *locally* constrained by a pure cohesive term, hence the need for the surface-activation term.

$(1-s)^2/l$, while the effect of $|\nabla s|^2$ is that of penalizing the transition between the zones $s=1$ and $s=0$. The optimal condition is achieved when the region $s=0$ concentrates in thin bands, so to produce a localized compliance that can release the whole body. The last term of (2.4) implies an energy consumption in the region where $s<1$, proportional to the norm of the displacement gradient. This indicates that the work to be done is a linear function of the strain increase on the glide band.

It is proved in [21] that, as $l \to 0$, provided that o_l is an infinitesimal faster than l, the regularized problem (2.3) $\Gamma-$converges to the strong formulation (2.2) and (2.1). Thinking of this limit, in any simulation that makes use of the weak formulation it is customary to consider very small values of o_l (in the following we will assume o_l of the order 10^{-5}). The presence of this term implies that there is a residual non-zero elastic-stiffness in the completely damaged material but this effect, for the aforementioned reasons, is not considered relevant.

In terms of plastic deformation, the sharp surfaces of discontinuity for the displacement field that characterize the strong formulation become slip bands of thickness of the order of l in the regularized weak formulation, where the displacement field exhibits a very high, but finite, gradient. Therefore l is an important parameter that represents the material intrinsic length scale [28]. This is why the regularized formulation should not be considered just a mathematical "trick" to approximate sharp discontinuities in the displacement field. Indeed, it provides a view of the phenomenon closer to reality than the strong formulation, as corroborated by experiments on metallic alloys and other materials, showing that yielding is characterized by strain localization in bands of small, but finite, width.

2.2. Regularized formulation in plane strain or generalized plane stress

Let now Ω represent the undistorted reference configuration of a body in plane strain (or generalized plane stress) and let $\mathbf{u}:\Omega\to\mathbb{R}^2$ indicate the *in-plane* displacement field (or its average-in-the-thickness, supposed small). Using a procedure formally similar to that used

in [28, Sect. 3.3], the regularized formulation of (2.3) and (2.4) can be extended to this case as

$$\min_{\mathbf{u}\in\bar{\mathcal{A}}} \mathcal{E}_l(\mathbf{u},s)\ ,\ \ \bar{\mathcal{A}} = \{(\mathbf{u},s)\in W^{1,2}(\Omega,\mathbb{R}^d)\times W^{1,2}(\Omega,\mathbb{R}) : \mathbf{u}=\bar{\mathbf{u}}\,\text{and}\,s=1\,\text{on}\,\partial\Omega^{\mathcal{D}}\}\,, \quad (2.5)$$

where the energy functional $\mathcal{E}_l(\mathbf{u},s)$ is composed of three terms, i.e.,

$$\mathcal{E}_l(\mathbf{u},s) = \mathcal{E}_{elast}(\mathbf{u},s) + \mathcal{E}_{act,l}(s) + \mathcal{E}_{plast}(\mathbf{u},s)\,. \quad (2.6)$$

Here $\mathcal{E}_{elast}(\mathbf{u},s)$ is the energy associated with *elastic* straining; $\mathcal{E}_{act,l}(s)$ is representative of the surface-*activation* energy, necessary to unpin the slip surface; finally, $\mathcal{E}_{plast}(\mathbf{u},s)$ indicates the work dissipated into plastic slip. Denoting with ∇^s the symmetric part of the gradient operator ∇, analogously to (2.4), one will define

$$\mathcal{E}_{act,l}(s) = \frac{\gamma}{2}\int_\Omega \left(l|\nabla s|^2 + \frac{(1-s)^2}{l}\right) d\mathbf{x}\,, \quad (2.7)$$

and

$$\mathcal{E}_{plast}(\mathbf{u},s) = \sigma_0 \int_\Omega (1-s)^2\,|\nabla^s\mathbf{u}|\,d\mathbf{x}\,. \quad (2.8)$$

There is clearly an energetic competition between the elastic energy stored inside the material, on the one side, and the energy necessary to nucleate new slip surfaces and dissipated during plastic slip, on the other side. Indeed, The term $\mathcal{E}_{elast}(\mathbf{u},s)$ represents the energy associated with *elastic* straining, from which comes the driving force for the occurrence plastic slip. Different in type models can be obtained while varying the form of this term, while maintaining fixed the expressions given by (2.7) and (2.8).

2.2.1. Phase-field model for plastic cleavage bands

Assume, as in [25], that the elastic part of the energy takes the form

$$\mathcal{E}_{elast}(\mathbf{u}, s) = \frac{1}{2}(s^2 + o_l)\mathbb{C}\left[(\nabla^s \mathbf{u})\right] \cdot (\nabla^s \mathbf{u})\,, \tag{2.9}$$

where $\mathbb{C} : Sym \to Sym$ denotes the elasticity tensor of the sound material and, again, o_l is an infinitesimal faster than l. For $l \to 0$ no $\Gamma-$convergence result is yet available, to our knowledge, for the minimization problem (2.5) of the functional defined by (2.6), (2.7), (2.8) and (2.9). Nevertheless, we are interested in this model *per se*, without any need for a legitimation by a theorem of variational convergence.

The stress tensor $\mathbf{T}$, dual in energy with respect to the strain $\nabla^s \mathbf{u}$, reads

$$\mathbf{T} = (s^2 + o_l)\mathbb{C}\left[\nabla^s \mathbf{u}\right] + \sigma_0(1-s)^2 \frac{\nabla^s \mathbf{u}}{|\nabla^s \mathbf{u}|}\,. \tag{2.10}$$

Since in general it is assumed that $o_l \ll 1$, modulo the effect of o_l when $s = 1$ one obtains the stress in the pristine elastic material, whereas when $s = 0$ the stress is proportional to $\nabla^s \mathbf{u}$ and its norm is equal to σ_0. Moreover, one can demonstrate [25] that the regions where $s \to 0$ tends to concentrate in bands of thickness of the order of l [28], where the strain localizes ($|\nabla^s \mathbf{u}|$ becomes very large). There is no restriction in this theory on the principal components of strain in the yielded zone and, in particular, the normal component of strain in the direction orthogonal to the slip band can become very large. In the language of fracture mechanics this is equivalent to the "opening" in mode-I of a plastic band and hence this approach could be referred to as phase field model for plastic *cleavage* bands.

Although the kinematics of deformation that can be obtained with this model is against the assumption that plastic flow is due to pure slipping along thin bands, the analysis of paradigmatic examples, considered in [25], provides solutions in agreement with the classical continuum plasticity theory. The reason is that the continuum theory can only furnish an

average view of the plastic deformation, independently of the phenomena occurring at the micro/mesoscopic level from which it originates.

2.2.2. Phase-field model for plastic slip bands

Consider now the case in which the elastic part of the energy takes the form

$$\mathcal{E}_{elast}(\mathbf{u}, s) = \frac{1}{2}\mathbb{C}\left[(\nabla^s \mathbf{u})_{sph}\right] \cdot (\nabla^s \mathbf{u})_{sph} + \frac{1}{2}(s^2 + o_l)\mathbb{C}\left[(\nabla^s \mathbf{u})_{dev}\right] \cdot (\nabla^s \mathbf{u})_{dev}\,, \tag{2.11}$$

where, indicating with $\mathrm{Tr}(\cdot)$ the trace operator,

$$(\nabla^s \mathbf{u})_{sph} = \frac{1}{3}\mathrm{Tr}(\nabla^s \mathbf{u})\mathbf{I}\,, \quad (\nabla^s \mathbf{u})_{dev} = \nabla^s \mathbf{u} - (\nabla^s \mathbf{u})_{sph}\,, \tag{2.12}$$

represent the spherical and deviatoric part of the infinitesimal strain tensor, respectively.

Suppose that $\mathbb{C}[(\nabla^s \mathbf{u})_{sph}]\cdot(\nabla^s \mathbf{u})_{dev} = \mathbb{C}[(\nabla^s \mathbf{u})_{dev}]\cdot(\nabla^s \mathbf{u})_{sph} = 0$, as in the case of an isotropic elastic solid. Then, the driving force for plastic yielding is directly related, as in classical von Mises'criterion of plasticity, to the deviatoric strain energy term. The corresponding stress tensor reads

$$\mathbf{T} = (s^2 + o_l)\mathbb{C}\left[(\nabla^s \mathbf{u})_{dev}\right] + \mathbb{C}\left[(\nabla^s \mathbf{u})_{sph}\right] + \sigma_0(1-s)^2\frac{\nabla^s \mathbf{u}}{|\nabla^s \mathbf{u}|}\,. \tag{2.13}$$

Modulo the infinitesimal o_l, again one recovers the stress in the pristine elastic material when $s = 1$, but observe that, on the contrary of (2.10), when $s = 0$ the stress is not any more bounded for $|\nabla^s \mathbf{u}| \to +\infty$. Indeed, only the deviatoric part of the elastic strain energy of (2.11) is multiplied by the field parameter s^2, and consequently, on a slip band, only the deviatoric part of $\nabla^s \mathbf{u}$ is allowed to grow with negligible energy consumption, whereas the energetic contribution of the spherical part remains unaffected. Therefore, the preferred straining for the material on the slip bands is a shear strain with small dilatation, i.e., the two faces in contact with the band undergo a plastic slip.

To illustrate in more detail, let the rectangle $\Omega = \{-d/2 \leq x_1 \leq d/2\} \times \{-h/2 \leq x_2 \leq h/2\}$ denote the undistorted reference configuration of a body in plane strain, of the same type represented later on in Figure 9. Indicating with $(\mathbf{e}_1, \mathbf{e}_2, \mathbf{e}_3)$ the unit vectors associated with the reference system (x_1, x_2, x_3), let the body be subject to the tractions *per* unit area $t\,\mathbf{e}_1$ on the face $x_2 = h/2$ and $-t\,\mathbf{e}_1$ on $x_2 = -h/2$. Supposing $h > d$, consider the formation of a slip band whose width is of the order of $l \ll d$, so that $s \simeq 0$ in the band and $s \simeq 1$ outside the band. As a zero order approximation, the state of strain in the yielded portion is supposed to be of the form $\nabla^s \mathbf{u} = \varepsilon_1 \mathbf{e}_1 \otimes \mathbf{e}_1 + \varepsilon_2 \mathbf{e}_2 \otimes \mathbf{e}_2$, with ε_1 and ε_2 constants to be determined.

If the material is elastically homogeneous and isotropic, denoting with λ and μ the Lamé constants so that $\mathbb{C} = \lambda \mathbf{I} \otimes \mathbf{I} + 2\mu \mathbb{I}$, for $s = 0$ and $o_l \to 0$, the state of stress (2.13) results to be of the form

$$\mathbf{T} = \kappa(\varepsilon_1 + \varepsilon_2)(\mathbf{e}_1 \otimes \mathbf{e}_1 + \mathbf{e}_2 \otimes \mathbf{e}_2 + \mathbf{e}_3 \otimes \mathbf{e}_3) + \frac{\sigma_0}{\sqrt{\varepsilon_1^2 + \varepsilon_2^2}} + (\varepsilon_1\,\mathbf{e}_1 \otimes \mathbf{e}_1 + \varepsilon_2\,\mathbf{e}_2 \otimes \mathbf{e}_2)\,, \quad (2.14)$$

where $\kappa = \lambda + \frac{2}{3}\mu$ is the Kelvin's modulus. Equilibrium with the external applied loads for one of the two parts of the body split by the band or, equivalently, equilibrium at the interface, gives conditions

$$\kappa(\varepsilon_1 + \varepsilon_2) + \frac{\sigma_0\,\varepsilon_1}{\sqrt{\varepsilon_1^2 + \varepsilon_2^2}} = 0\,, \quad \kappa(\varepsilon_1 + \varepsilon_2) + \frac{\sigma_0\,\varepsilon_2}{\sqrt{\varepsilon_1^2 + \varepsilon_2^2}} = t\,. \quad (2.15)$$

By defining $a = (\varepsilon_2 - \varepsilon_1)$ and $\varrho^2 = (\varepsilon_1^2 + \varepsilon_2^2)$, so that $(\varepsilon_1 + \varepsilon_2)^2 = 2\varrho^2 - a^2 > 0$, one finds from (2.15)

$$\sigma_0 \frac{a}{\varrho} = t \;\; \Rightarrow \;\; (\varepsilon_1 + \varepsilon_2)^2 = \varrho^2 \left(2 - \frac{a^2}{\varrho^2}\right) = \varrho^2 \left(2 - \frac{t^2}{\sigma_0^2}\right) \geq 0\,, \quad (2.16)$$

from which it follows that $|t| \leq \sqrt{2}\sigma_0$. Therefore, there is an upper bound for the applied stress.

Moreover, one finds that

$$\varrho = \frac{\sigma_0}{2\,\kappa}\frac{|t|/\sigma_0 - \sqrt{2-(t/\sigma_0)^2}}{\sqrt{2-(t/\sigma_0)^2}}\,,\quad a = \frac{t}{2\,\kappa}\frac{|t|/\sigma_0 - \sqrt{2-(t/\sigma_0)^2}}{\sqrt{2-(t/\sigma_0)^2}}\,, \tag{2.17}$$

which is well defined when $\sigma_0 < |t| < \sqrt{2}\sigma_0$. Besides

$$\varepsilon_1 + \varepsilon_2 = \frac{t}{|t|}\sqrt{2\varrho^2 - a^2} = \frac{t}{|t|}\frac{\sigma_0}{2\,\kappa}\left(|t|/\sigma_0 - \sqrt{2-(t/\sigma_0)^2}\right)\,. \tag{2.18}$$

Therefore, $|\varepsilon_2| > |\varepsilon_1|$ and when $t > 0$ ($t < 0$) then $\varepsilon_2 > 0$, $\varepsilon_1 < 0$ ($\varepsilon_2 < 0$, $\varepsilon_1 > 0$).

Moreover, observe that when $|t| \to (\sqrt{2}\,\sigma_0)^-$, one obtains from (2.17) and (2.18) that $a \to \infty$, $\varrho \to \infty$ and $2\varrho^2 - a^2 \to \frac{1}{2}\sigma_0^2/\kappa^2$, or equivalently, $|\varepsilon_1 - \varepsilon_2| \to \infty$ and $(\varepsilon_1 + \varepsilon_2)^2 \to \frac{1}{2}\sigma_0^2/\kappa^2$. In words, the band tends to be inclined at 45^o and inside it the deformation is *approximately* an unbounded pure shear. The band is *exactly* inclined at 45^o and the deformation is pure shear in the limit $\kappa \to \infty$.

Where $s \simeq 0$, the strain in the direction of the band tends to

$$\varepsilon^0_{45} = \frac{\varepsilon_1 + \varepsilon_2}{2} \to \frac{t}{|t|}\frac{\sqrt{2}\sigma_0}{4\,\kappa}\,. \tag{2.19}$$

On the other hand, in the unyielded portion where $s = 1$, the strain of fibers inclined at 45^o can be calculated assuming that, here, the stress is $\mathbf{T} = t\,\mathbf{e}_2 \otimes \mathbf{e}_2$, so that for $|t| \to (\sqrt{2}\,\sigma_0)^-$, to give

$$\varepsilon^1_{45} = \frac{\varepsilon_1 + \varepsilon_2}{2} = \frac{t}{4(\lambda+\mu)} = \frac{t}{4(\kappa + \frac{1}{3}\mu)} \to \frac{t}{|t|}\frac{\sqrt{2}\sigma_0}{4(\kappa + \frac{1}{3}\mu)}\,. \tag{2.20}$$

Therefore, in general there is a strain mismatch at the interface between the yielded band and the unyielded portion, which should be accommodated at the price of elastic straining thus defining a transition zone with $0 < s < 1$. However, it must be observed from (2.19) and (2.20) that in the limit in which the elastic moduli tend to infinity, such mismatch vanishes.

In this case the material is rigid-plastic and the resulting deformation coincides with that predicted by classical slip-line field theory.

As a final remark, notice that problems of the type (2.5) do not make any distinction between tension and compression, in the sense that by reversing the sign of the boundary data one obtains exactly the same plastic-band pattern. In fact, the energy functionals to be minimized remain unaltered by changing the sign of $\nabla^s \mathbf{u}$, whatever the expression of the elastic contribution, either (2.9) or (2.11), is. In principle, neither the cleavage-band model nor the slip-band models are able to avoid material interpenetration on a plastic line, but whereas in the former the whole infinitesimal strain tensor can grow unboundedly where $s = 0$, the latter allows only the deviatoric part to explode, preserving the full elastic strain energy associated with the hydrostatic part of the strain. In the language of fracture mechanics, the model derived from (2.9) allows for mode-I plastic bands, whereas using (2.11) the bands can slip in mode II. The possibility of material interpenetration on a mode-II plastic band is mitigated, being possible only in the case of extreme spherical deformations, which are limited by the fact that the corresponding elastic strain energy remains unaffected by the field s.

2.3. Numerical implementation

The minimization problem (2.5) is numerically solved using an incremental procedure analogous to that proposed in [25]. Firstly the quasi-static evolution of the problem is discretized in time. Let the non-dimensional loading (and time-like) parameter t be increased from 0 to the final value T with N finite increments of amplitude $t_0 = T/N$. Accordingly, $\mathbf{u}_t$ and s_t represent the displacement and damage field evaluated at time t respectively.

At each time step the minimization of (2.5) requires a discretization in space. Due to non-convex nature of the problem the implemented numerical scheme is based upon an alternate minimization algorithm which, in short, consists in solving for each time-step t a series of minimization sub-problems on $\mathbf{u}$ at fixed s and, viceversa, on s at fixed $\mathbf{u}$ up to convergence.

Moreover, a further condition must be considered which accounts for the irreversibility of the yielding process, equivalent to the requirement that s cannot increase with t. Since evolution is evaluated numerically at discrete steps, the condition becomes

$$s_t(\mathbf{x}) \leqslant s_{t-t_0}(\mathbf{x}) \ , \ \forall \mathbf{x} \in \Omega \, . \tag{2.21}$$

Numerical details concerning the numerical treatment can be found in [25]. The minimization problem is numerically solved using a finite element method, implemented in an appositely conceived program based upon the Open Source package deal.II [29].

An accurate finite element treatment of the phase-field formulations of fracture is computationally demanding task in two or three dimensions. The need to resolve the small length-scale l implies extremely fine meshes, at least locally in the transition or totally damaged zones. A robust and efficient fully adaptive mesh refinement strategy for phase field formulation is far from being consolidated. Traditional estimators based on adaptive mesh refinement schemes are not appropriate. In fact, an alternative predictor-corrector scheme for local mesh adaptivity to reduce the computational cost was recently proposed in [30] for pressurized fracture. Moreover, the path of crack evolution can be strongly influenced by the choice of the refinement algorithm and the parameters in the adaptive algorithm as indicated in [31]. Again, the crack path can also be influenced by mesh orientation and anisotropy [32] thus generating spurious solutions characterized by unrealistic crack paths.

In this work the main focus is the determination of the slip lines in a smeared approach. So, in order to limit the drawbacks previously described a uniform structured mesh has been adopted for the numerical examples. Quadrilateral four nodes finite elements with linear shape function have been considered in the numerical simulations. The size of the finite element has been chosen smaller than l, to correctly determine the width of the transition zone and to avoid influence on the crack paths.

3. Numerical experiments

In this section two paradigmatic numerical experiments will be illustrated. The first one will reproduce the compression test of a lamina, while the second one represents a pipe line under internal expansion.

3.1. Compression of a lamina

In a number of important practical problems, such as drawing, extrusion, indentation, and piercing, the unrestricted plastic flow begins while the body is still partially plastic. In such cases, the elastic strain becomes soon negligible throughout the plastic zone except in a certain transition region bordering the elastic zone. If the transition region is sufficiently narrow, no significant error is introduced by neglecting the elastic strains. It is therefore a reasonable approximation to regard the material as rigid-plastic for the determination of the stress and velocity distributions in the plastically deforming region. For such cases, classical slip-line theory is an effective instrument to determine the surfaces of plastic flow. The analysis determines plane-strain deformation fields that are both geometrically self-consistent and statically admissible and, therefore, they correspond to exact solutions.

One classic example is the compression between rigid platens of a rectangular solid in plane strain or generalized plane stress. This setup approximates conditions during hot forging, when a rectangular block of material is compressed symmetrically by a pair of rigid parallel platens under conditions of plane strain. The numerical experiment reproduces the loading conditions depicted in Figure 1 for a specimen geometry with height H and width L.

The problem is traditionally solved by using slip-line field theory for both cases of compression between rough (sticky) platens and smooth (slippery) platens. The two solutions substantially differ one another and both depend upon the ratio L/H, so that different geometric dimensions of the specimen have been considered. The element is loaded by applying a vertical displacement on the upper base, while the lower base is kept fixed and the two vertical borders are unconstrained and traction free. The horizontal displacement of both

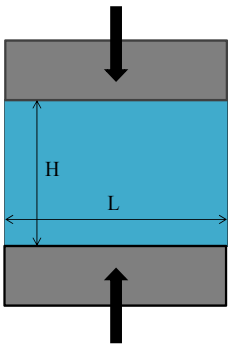

Figure 1: Schematic representation of the compression of a rectangular solid.

the lower and upper bases is kept fixed in the case of rough sticky platens, whereas the specimen is left free to laterally expand when in contact with smooth slippery platens.

The problem is here solved by using the phase field model for plastic slip bands defined by (2.5), where the energy functional is provided by (2.6), (2.7) and (2.8), being the elastic contribution of the type (2.11). The material properties adopted for the simulations are listed in Table 1. The boundary conditions in terms of tractions and displacement are immediately recognizable. For what the field s is concerned, the natural conditions from the variational problem imply that on the two vertical free surfaces the derivative of s in the direction of the outward unit normal is null, whereas on the horizontal basis we impose $s = 1$. The latter requirements and its physical interpretation have been discussed in [33] and [25].

E (MPa)	ν	γ (N/mm)	l (mm)	σ_0 (MPa)
210000	0.3	2.5e-2	2.5e-2	120

Table 1: Material parameters used in the numerical experiments of the compression of a rectangular solid.

In the numerical discretization, a structured and homogeneous mesh composed by quadrilateral finite element with size equal to $0.25l$ has been used.

3.1.1. Rough (sticky) platens

Consider the compression between rough platens for a rectangular specimen with different geometric ratio L/H. The analytic solution provided by slip-line field theory as *per* [34] is

outlined in Figure 2, where the slip-lines are plotted for increasing values of L/H. Zones of plastic material are always initiated at the corners of the platens. Since the material is rigid/plastic, the platens cannot approach one another until the plastic zones have spread through the whole block, to form an admissible kinematic mechanism. When the yield point is attained, the plastic compression of the block begins, and the rigid overhangs are thrust apart.

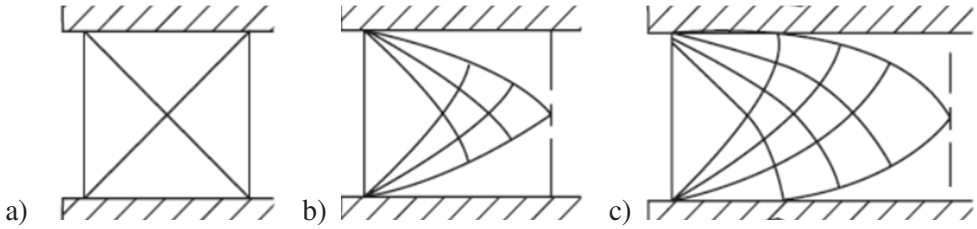

Figure 2: Slip line field for the compression of a rectangular block between parallel rough (sticky) platens, as indicated in [34]. Cases: a) $L/H = 1$; b) $L/H \simeq 2$; c) $L/H \simeq 4$.

In particular, for the square specimen of Figure 2a, the slip-line field assumes the classical criss-cross path. For longer specimen, the slip-line field presents curved paths (Figure 2b). The slip lines are always parallel and perpendicular to the platens and there are two dead (inactive) zone, approximatively triangular, in proximity of the free edges. Two central rigid regions delimited by the plate borders move down with the platen, losing material to the plastic region as the compression proceeds. The triangular region at the sides of the block is then uniformly stressed to the yield point, and is moved outward as a rigid block. For extremely long specimen the slip lines meet the platens tangentially over a certain length, showing the recurring behaviour represented in Figure 2c.

Numerical computations have been performed for values of the ratio $H/L = 1$, 4 and 8, while maintaining fixed the height $H = 50$ mm. Figures 3, 4 and 5 summarize the damage evolution obtainable for the different geometric ratios.

Figure 3 represents the evolution of the damage field $s(\mathbf{x})$ predicted by the model for increasing values of vertical displacement in the case of a square $H/L = 1$. The slip band field, where the deformation localizes, is represented by the locus of points where $s \simeq 0$. The path

is typical of specimens subject to shear band failure mode. Two x-shaped shear bands are nucleates (Figure 3a) where deformation strongly localizes; as the compression increases the width of the bands also increases, as indicated in Figure 3b as the compression increases. The numerical result clearly is in agreement with the analytic solution. However, here we can notice the formation of partially yielded zones, which widen as the platens become closer. This is due to the fact that in the proposed theory the material is not rigid but elastically deformable. Partial yielding is indicated by values of the variable s that are intermediate between zero and one.

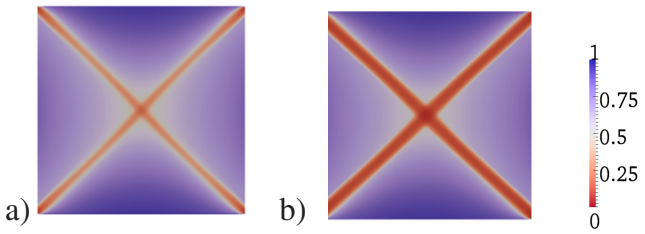

Figure 3: Quadratic specimen ($H/L = 1$) compressed by rough (sticky) platens. Evolution of the field s when the distance between the platens is diminished.

For the case $H/L = 4$, the evolution of the slip lines is much more complex, as indicated in Figure 4. Since the material is not rigid in the unyielded condition, the nucleation of slip lines is not instantaneous but occurs gradually as the relative distance between the loading platens is diminished. In particular, in the loading history considered here, four new curvilinear slip-lines initiate and start propagate at different compression levels. The solution is again in substantial agreement with the analytic predictions, even if a difference can be noticed in the triangular regions where no rectilinear slip-line, but rather a diffuse plasticization takes place and progresses towards the free, traction-free, borders. Increasing the compression, the characteristic inclination of $\pi/4$ of the rectilinear slip-lines that delimit the extreme triangular portions can be reconciled through the increase in the width of the bands, as outlined in Figures 4d-e.

For a very long specimen, the extreme slip lines present no longer an inclination of $\pi/4$ with respect to the loading plates. As represented in Figure 5, where the rectangular specimens

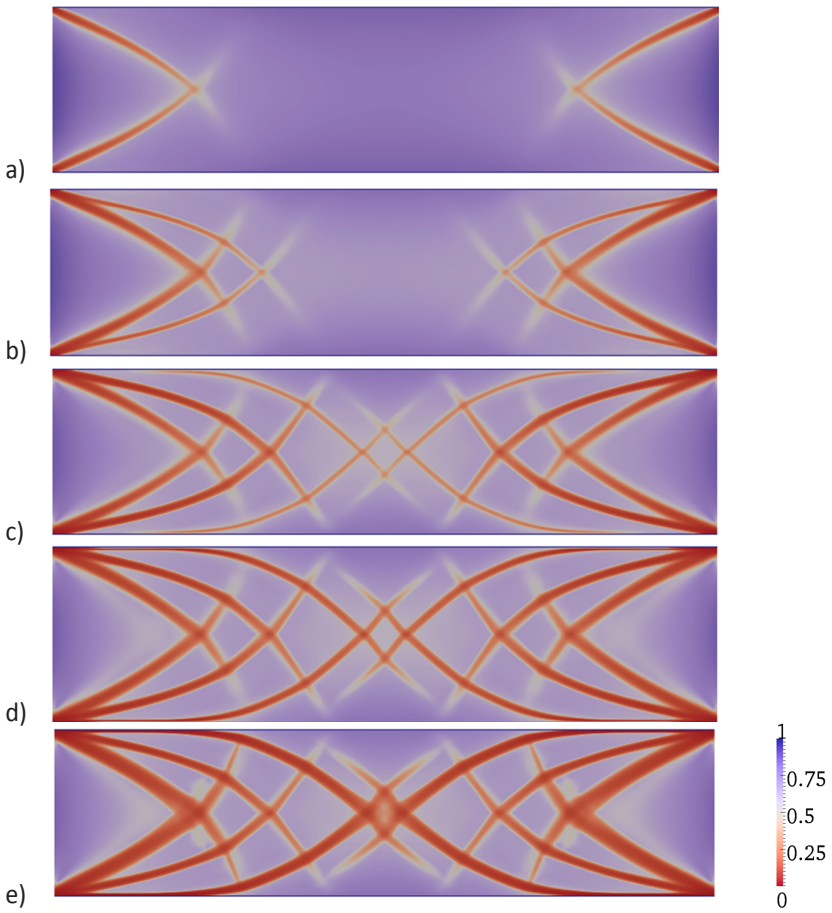

Figure 4: Rectangular block ($H/L = 4$) compressed by rough (sticky) platens. Evolution of the field s when the distance between the platens is diminished.

are rotated of 90^o for convenience of representation, the slip bands are progressively nucleated starting from the extremities, and gradually progress towards the center of the specimens. Partially yielded regions smoothly fit with the bands where the strain localizes. In any case, there is again a good accordance with the analytic solution.

3.1.2. Smooth (slippery) platens

If there is no tangential component of stress at the interface between the material and the plates (slippery platens condition), a very simple analytic solution for the compression problem can be obtained in the limit $L/H \to \infty$. As illustrated in Figure 6, the block results divided into a number of independent rigid units identified by a symmetrical criss-

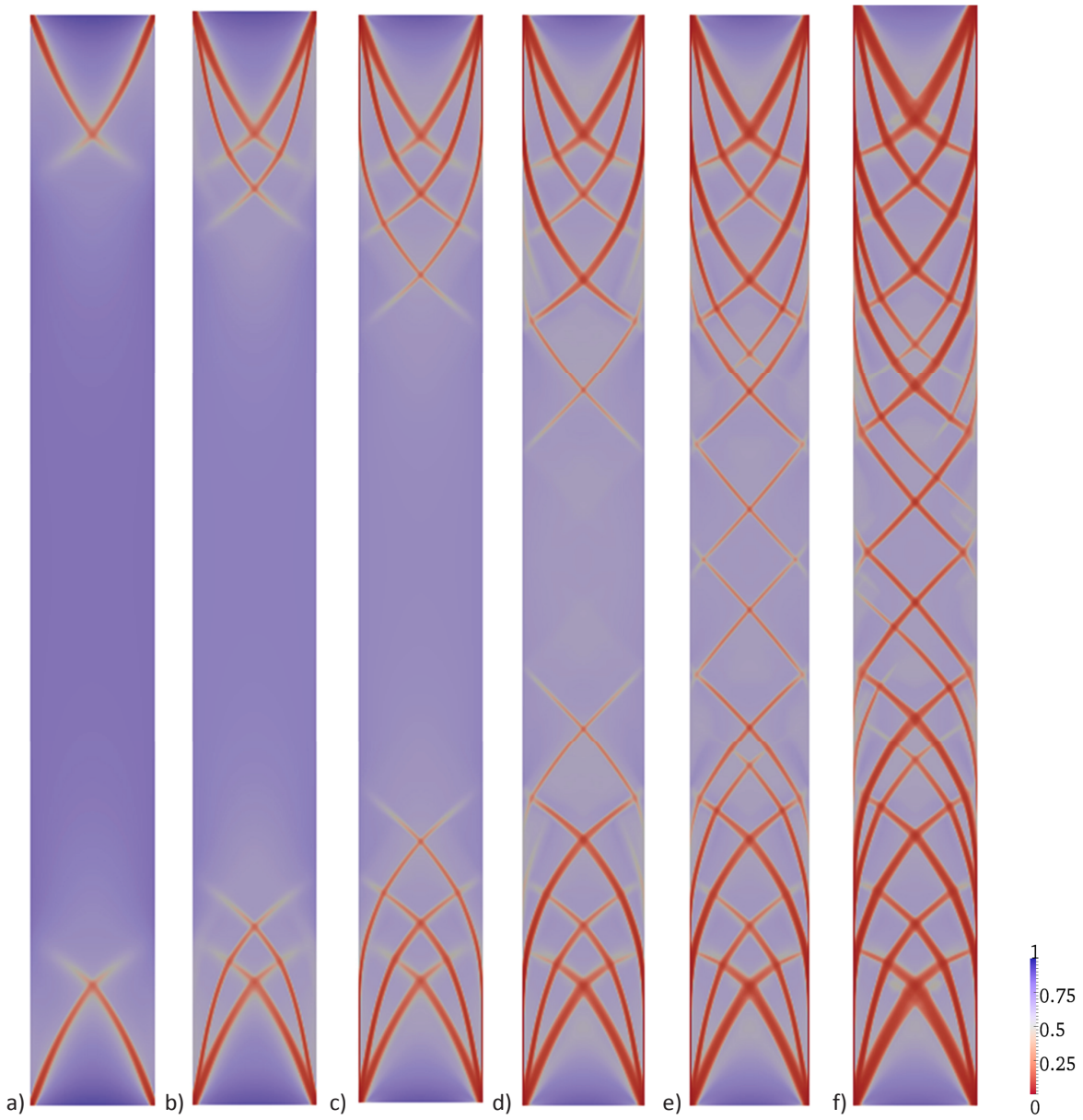

Figure 5: Elastic plastic block in the shape of an elongated rectangle ($H/L = 8$) compressed by rough (sticky) platens. Evolution of the field s when the distance between the platens is diminished.

cross system of slip lines inclined, at a constant acute angle θ, with respect to the plane of the platens.

For a block of finite length the solution is slightly more complex. As represented in Figure 7, taken from [35], the system of slip lines is similar to that associated with the limit condition,

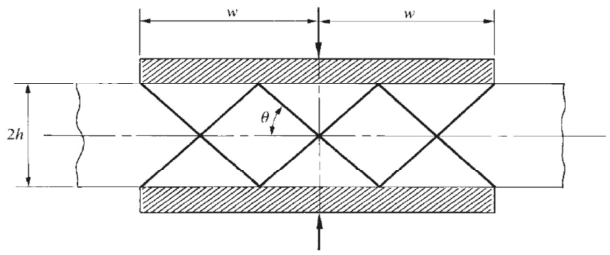

Figure 6: Slip-line field for frictionless compression of a very long block. Limit solution for $L/H \to \infty$ as *per* [34].

but the lines results slightly curved.

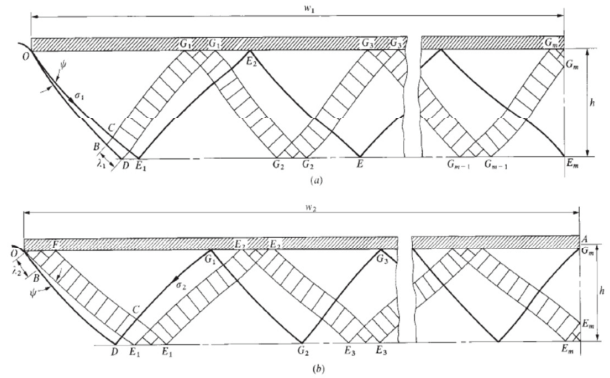

Figure 7: Slip-line field for frictionless compression of a block of finite length L. Two general solutions for different values of the ratio L/H [35].

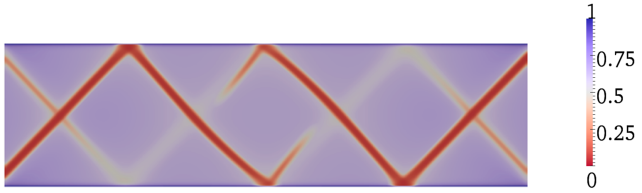

Figure 8: Elastic plastic block $H/L = 4$ compressed by smooth (slippery) platens. Evolution of the field s when the distance between the platens is diminished.

The numerical solution obtained with the proposed approach for the case $L/H = 4$ is represented in Figure 8. It is characterized by a pattern of the plastic bands in excellent accordance with the analytic solutions. However, even if symmetry with respect to the middle axis parallel to the platens is lost, the numerical solution exhibits rectilinear slip-

lines at the extremities, while the inner slip-lines are characterized by curvilinear paths. Only one family of the expected slip-lines is fully developed; the second family is nucleated after this, when the displacement at the boundary is increased. The numerical solution, that corresponds to a local minimizer for the energy, resumes both the aforementioned analytic solutions of Figures 6 and 7.

3.2. Expansion of a pipe line under applied internal pressure

This problem is suggested by a very practical application. Large-diameter pipes, extensively used in offshore applications and oil pipelines, are commonly manufactured by cold-forming plates through the UOE process. The plate is crimped along its edges, formed into a U-shape and then pressed into an O-shape between two semicircular dies. Then the pipe is welded closed and then circumferentially expanded to obtain a highly circular shape. Collapse experiments have demonstrated that these steps, especially the final expansion, can degrade the mechanical properties of the pipe and result in a reduction in its collapse pressure upwards of 30% [36]. Recent researches have attributed such a degradation of mechanical properties to the Bauschinger effect and the work hardening during UOE forming process, which modify the yield strength of the UOE pipe with respect to that from pristine steel plates [37].

However, the question arises whether the traditional model of plasticity is able to represent the complex phenomena that occur during the cold forming process, especially the radial expansion. If the equations of the mathematical plasticity theory are applied to a long hollow cylinder in plane strain subjected to internal pressure, one derives that the plasticization of the tube is progressive and is represented by a radially symmetric flow gradually invading the whole cross section of the tube (see, e.g., [2], Sect. 30). However, the type of plasticization predicted by slip line theory is completely different, being the slip lines two orthogonal families of logarithmic spirals ([2], Sect. 37). Understanding the real mechanism of deformation and the resulting state of stress is of crucial importance to detect the critical steps in the production process.

Here, we apply the proposed model to the case of a circular pipe under internal pressure, starting from the characterization of material properties that could be obtained by means of an uniaxial traction test. Then, a comparison is made between the results obtainable either by applying the model for plastic cleavage bands, associated with the elastic strain energy (2.9), or the model for slip bands, characterized by the deviatoric specialization of the energy functional as *per* (2.11).

3.2.1. Material Characterization

The model is here applied to reproduce the mechanical characterization of the material properties by means of uniaxial tensile tests. The test setup shown in Figure 9 represents a prismatic body, supposed for simplicity in plane strain condition, whose section of sides d and h is denoted with Ω. The element is loaded by applying a vertical displacement on the upper base Γ_2, while the lower base Γ_1 is kept fixed, not impeding the lateral contraction; the vertical borders Γ_3 and Γ_4 are unconstrained and traction free. Moreover, as discussed in [25], we set $s = 1$ on Γ_1 and Γ_2. In summary, the boundary conditions for this problem read

$$\begin{cases} \mathbf{u} \cdot \mathbf{e}_2 = 0, \ \mathbf{T}\mathbf{e_2} \cdot \mathbf{e}_1 = 0, \quad s = 1, \quad \text{on}\, \Gamma_1\,, \\ \mathbf{u} \cdot \mathbf{e}_2 = u, \quad \mathbf{T}\mathbf{e_2} \cdot \mathbf{e}_1 = 0\,, \quad s = 1, \quad \text{on}\, \Gamma_2\,, \\ \mathbf{T}\mathbf{e}_1 = \mathbf{0}, \quad \nabla s \cdot \mathbf{e}_1 = 0, \quad \text{on}\, \Gamma_3 \text{ and } \Gamma_4\,, \end{cases} \tag{3.22}$$

where $\mathbf{e}_1$ and $\mathbf{e}_2$ are the horizontal and vertical unit vectors, respectively, u is the displacement parameter and $\mathbf{T}$ is the Cauchy stress tensor. The geometry of the specimen is $h = 100$ mm and $d = 30$ mm, while the mechanical parameters used in the numerical experiments are listed in Table 2.

E (MPa)	ν	γ (N/mm)	l (mm)	σ_0 (MPa)
210000	0.3	2.e-1	3.e-1	120

Table 2: Material parameters used in the numerical experiments for the expansion of a pressurized pipe.

The value of the energy functional (2.6) is plotted in Figure 9b as a function of the vertical displacement with distinction of the elastic part, represented by (2.9), the activation part (2.7) and the plastic part (2.8). Observe that the nucleation and propagation of slip bands is characterized by a transformation of the elastic energy into activation and plastic energy.

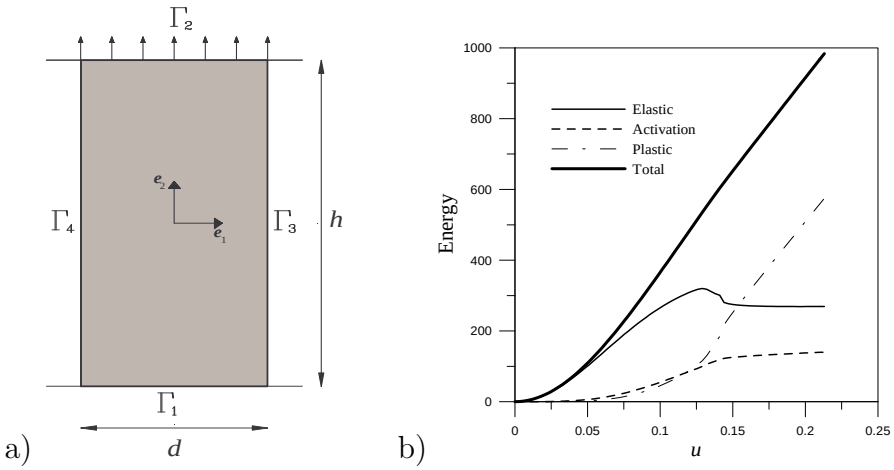

Figure 9: Uniaxial tensile dilatation. a) Section of the specimen in plain strain; b) energy diagram as a function of the applied dilatation with distinction of the elastic, activation and plastic parts.

The formation of the slip bands is represented in Figure 10 for three different values of the applied displacement: $u = 0.12$ mm, $u = 0.14$ mm and $u = 0.215$ mm. A classical criss-cross pattern is attained at the lower value of the considered displacement. Increasing the traction the width of one dominant band increases as well. To be noticed here is that the slip bands are not nucleated at the corners of the specimen, even if here some plasticity is clearly present. This may be attributed to the fact that, since the horizontal displacement is not constrained on the loaded bases (slippery platens conditions), the state of stress at the beginning of the loading history is uniform uniaxial, and there is no stress concentration at the corners. Consequently, the imposed Dirichlet condition s = 1 on Γ_1 and Γ_2 prevents, here, the formation of the band. On the other band, if the band was nucleated at the corner, there would be a conflicting deformation with the movement of the loaded bases, as indicated in [2], Chapter 15, Figure 15-19. It should also be observed that the bands are nucleated symmetric with respect to the horizontal mid-plane of the specimen and the axis of the

specimen. No other bands need to be nucleated because, once the glide surface is unpinned, it is energetically mode favorable to increase the plastic glide on one of them, rather than producing new surfaces of slip. This may give reasons why there is no reflection in the bands when the free boundary is met.

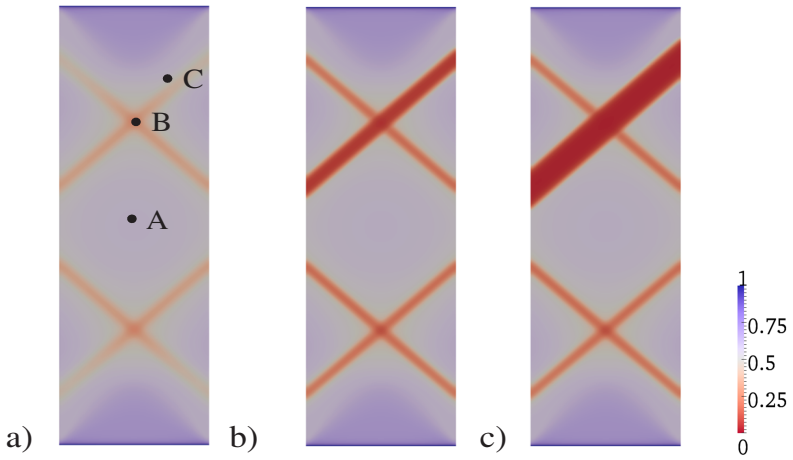

Figure 10: Uniaxial tensile dilatation. Formation of the slip bands for different values of the applied displacement: a) $u = 0.12$ mm; b) $u = 0.14$ mm; c) $u = 0.215$ mm.

The measured vertical load *per*-unit-thickness P is plotted in Figure 11a as a function of the vertical displacement u. One can observe a transition from an (pseudo) upper to a lower yield, after which the force asymptotically approaches a horizontal *plateau*.

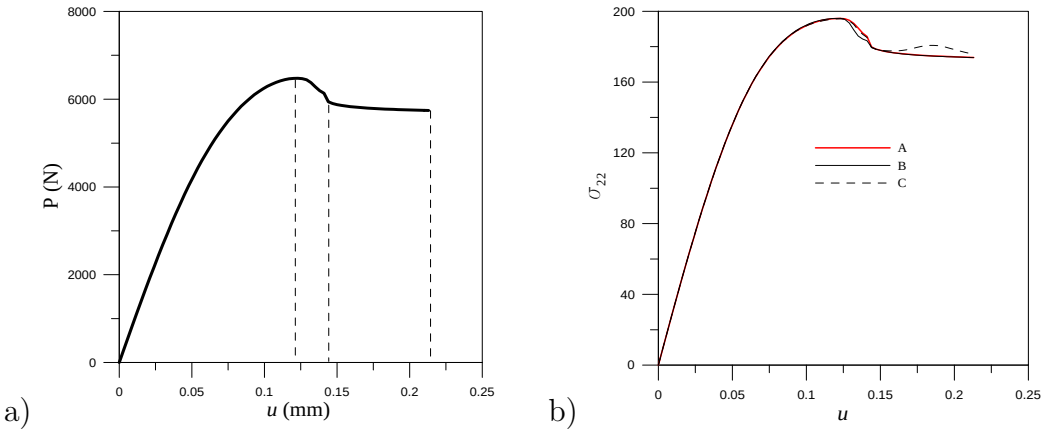

Figure 11: Uniaxial tensile dilatation. a) Vertical load *per* unit thickness P as a function of the corresponding vertical displacement; b) graph of the stress σ_{22} vs. u at points A, B, C of Figure10a.

The local response of the material has been also investigated at points A, B and C of Figure 10. In particular, point A is far from the yielded zone, point B is exactly in the plastic zone and point C is located in the process zone in a neighborhood of the band. In Figure 11b we report the stress σ_{22}, obtained from the numerical experiment, as a function of the vertical displacement u. At all the points the response is similar and is again characterized by a transition from an upper to a lower yield point, similar in type to the gross response of Figure 11a. It should also be observed that the peaks are reached in practice at the same time: there is a slight time shifting but, as in the classical slip-line theory, the formation of the bands is almost an instantaneous process during the loading history. By insight, such a strain localization is due to the fact that no material strain-hardening is included in the model. In fact, as discussed at length in [11, 38], strain-hardening represents the important feature that allows the orderly formation of multiple slip bands, gradually invading the bar as a plastic slow wave, associated with a pronounced plastic *plateau*.

3.2.2. Long pipe under internal pressure

Consider a long pipe for which a radial displacement u, dual in energy with the internal pressure p_i, has been applied along the inner surface. Due to the axial symmetry, we can consider just one quarter of the pipe, whose cross section is thus represented by a quarter of an annulus delimited by the orthogonal radial sections Γ_1 and Γ_2. Indicate with Γ_3 and Γ_4 the boundary arcs of circle corresponding to the inner and outer surfaces of the pipe, respectively, and suppose that an orthogonal reference system with origin at the center of the annulus is introduced, with corresponding unit vectors $\mathbf{e}_1$ and $\mathbf{e}_2$ such that $\mathbf{e}_1$ ($\mathbf{e}_2$) is normal to Γ_2 (Γ_1). If $\mathbf{e}_n$ denotes the outward unit normal to the external surface Γ_4, coinciding with the inward normal to Γ_3, and $\mathbf{e}_t$ is such that $\mathbf{e}_t \cdot \mathbf{e}_n = 0$, then the boundary conditions are of the type

$$
\begin{cases}
\mathbf{T}\,\mathbf{e}_2 \cdot \mathbf{e}_1 = 0, \quad \mathbf{u} \cdot \mathbf{e}_2 = 0, \quad \nabla s \cdot \mathbf{e}_2 = 0, \quad \text{on}\,\Gamma_1\,, \\
\mathbf{T}\,\mathbf{e}_1 \cdot \mathbf{e}_2 = 0, \quad \mathbf{u} \cdot \mathbf{e}_1 = 0, \quad \nabla s \cdot \mathbf{e}_1 = 0, \quad \text{on}\,\Gamma_2\,, \\
\mathbf{u} = u\,\mathbf{e}_n, \quad \mathbf{T}\,\mathbf{e}_n \cdot \mathbf{e}_t = 0, \quad \nabla s \cdot \mathbf{e}_n = 0, \quad \text{on}\,\Gamma_3\,, \\
\mathbf{T}\,\mathbf{e}_n = \mathbf{0}, \quad \nabla s \cdot \mathbf{e}_n = 0, \quad \text{on}\,\Gamma_4\,.
\end{cases}
\tag{3.23}
$$

The material parameters are taken from Table 2. In the considered case, the outer diameter D of the pipe is equal to 200 mm and the thickness t is 15 mm.

Figure12a shows the graph of the internal pressure p_i as a function of the radial displacement u. Similarly to the one dimensional dilatation of Figure 10, the pressure reaches a maximum upper value, then decreases, but no horizontal *plateau* is approached. Indeed, the response is strain softening in a test where the radial displacement is imposed, like the one considered here. Consequently, in a test where the internal pressure is gradually increased, the response would be almost linear up to the peak value, after which a brittle collapse would occur. This response is different in type to that predicted by classical plasticity theory, where the pressure vs. radial-displacement graph is always non-decreasing.

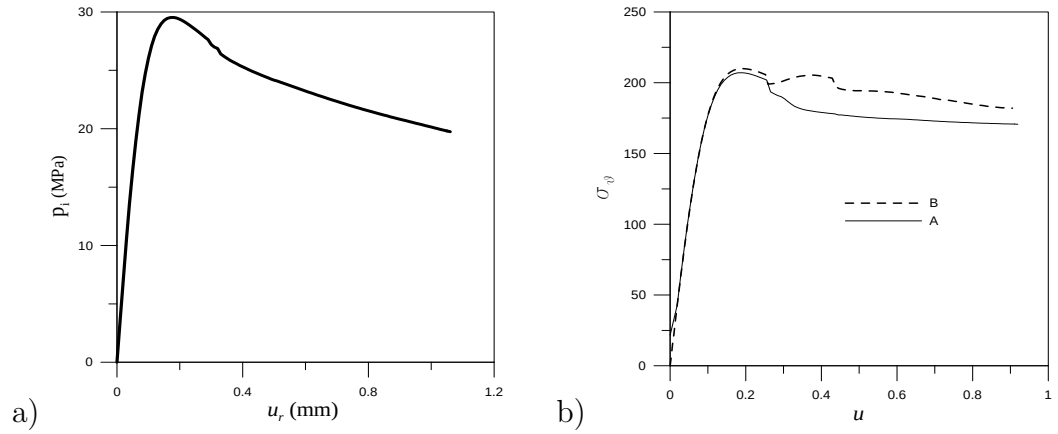

Figure 12: Expansion of a pipe line under internal pressure. a) Pressure p_i as a function of the corresponding radial displacement; b) graph of the hoop stress σ_θ as a function of the radial displacement u, evaluated at points A and B of Figure 13.

The map of the parameter s for the three different values of radial displacement $u = 0.3$, 0.35 and 0.4 mm is reported in Figure 13. Slip bands are formed that cross the whole pipe,

from the internal to the external surface. As the radial displacement increases, the thickness of the bands increases as well, and they tend to spread in the entire circular crown.

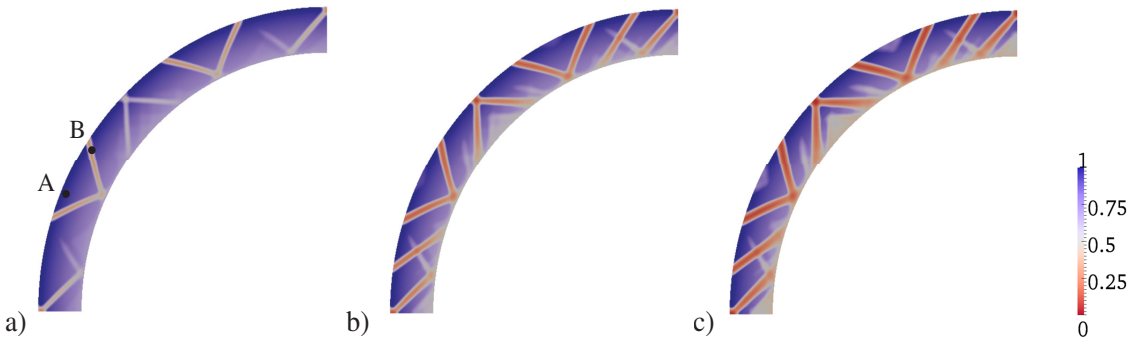

Figure 13: Expansion of a pipe line under internal pressure. Plot of the field s for different values of the radial displacement: a) $u = 0.3$ mm; b) $u = 0.35$ mm; c) $u = 0.4$ mm.

The local response of the material is investigated at the points A and B indicated in Figure 13a. Point A is located in an apparently neutral portion of the pipe, whereas point B is exactly on the slip band. In Figure 12b, the corresponding hoop stress component σ_θ is plotted as a function of the radial displacement u. Here the interpretation is more difficult than for the case of Figure 11b, because the state of stress if far from being uniaxial. In any case, observe that, as in the uniaxial dilatation, both the points are characterized by plastic deformations. Comparing with the graph of Figure 12a, observe that the gross response of the pipe is substantially different from the local response. This could also give reasons to explain the experimentally-verified pseudo-brittle response of the expanding pipe [37, 36].

Indeed, the embrittlement is associated with the strain-softening character evidenced in the pressure vs. displacement graph of Figure 12a, which is not caught by the classical theory for perfectly plastic materials. However, until the peak is not overcome, the classical theory furnishes a very good approximation. Using the maximum stress obtained in the uniaxial-dilatation experiment of Figure 11b, i.e., $\sigma_{max} = 195.82$ MPa, the application of Barlow's formula [39], usually adopted for pipe design, furnishes an allowable value of the maximum internal pressure $p_i^{max} = 2 \cdot \sigma_{max} \cdot t/D = 29.37$ MPa, which is in perfect agrement with the value 29.53 MPa found numerically.

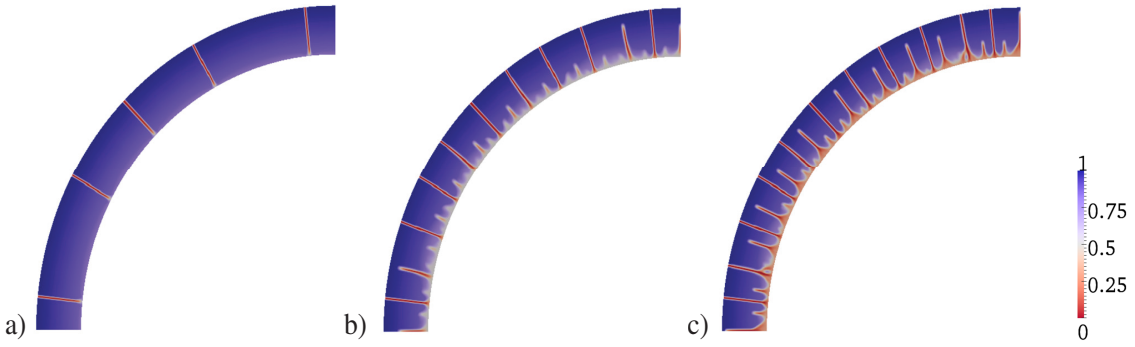

Figure 14: Expansion of a pipe line under internal pressure. Plot of the field s, obtained with the cleavage-band model, for different values of the radial displacement: a) $u = 0.3$ mm; b) $u = 0.35$ mm; c) $u = 0.4$ mm.

For the sake of comparison, the cleavage band model of Section 2.2.1 has also been applied to the same model. The pattern assumed by the plastic bands is represented in Figure 14, which is the counterpart of Figure 13. Now the development of the bands is purely radial, at right angle to the direction of the (maximal) hoop stress. At the beginning of the loading process just a few bands are produced (Figure 14a). Increasing the radial displacement, their number also increases (Figure 14b) and, eventually, they tend to coalesce (Figure 14c).

4. Conclusions

The proposed approach to plasticity is based upon an energetic competition between different-in-type deformation sources, which can be traced back either to a reversible distortion of bulk material portions, or to strain localization in narrow bands that, in the limit of infinitesimal thickness, can be treated as surfaces of slip. The resulting deformation is structured, in the sense that it is composed of a smoothly varying *elastic* part and the *plastic* part, characterized by very high displacement gradients localized in thin layers of slip. The problem has been treated with a "phase field" approach, following which an auxiliary field s (the *phase field*) is introduced, playing the role of an order parameter taking the 1 value on the elastic phase and the 0 value on the yielded phase. The location of the slip bands is thus defined as the set of points where s is null. The phase field is analogous to a damage field because the

material stiffness associated with the deviatoric part of the strain is annihilated as $s \to 0$. The main advantage of this approach is that all the unknowns are regular fields, so that numerical implementation is greatly facilitated.

The proposed formulation is substantially different from that of [25], because here plastic flow is driven by the deviatoric part of the strain energy only. This represents an alternative interpretation of von Mises' idea that plasticity affects the deviatoric part of the strain, being the changes in volume negligible with respect to the change in shape. The presence of an activation term in the energy functional allows for the possibility of attaining a pure elastic phase below the yield point. With respect to classical slip-line theory, the material comprised between the plastically deformed *lamellae* is not rigid. This implies that the energetic competition between plastic and elastic deformation is played at the *local* level. The proposed model thus permits the *gradual* plasticization of the body, because the transfer of energy from the elastic to the plastic part can occur in a whatever small portion, whereas in the classical rigid-plastic theory the whole slip-line pattern occurs instantaneously. In other words, whereas the classical slip-line method is essentially a limit-state theory, the proposed approach can describe all the phases of the yielding process. The proposed theory provides a better description of the structured nature of plastic deformation than the classical continuum theory of plasticity, because it can keep track of shear localization. Remarkably, there is also a scale-parameter that governs width of the developing bands, which represents the intrinsic material-length-scale.

A numerical code has been implemented to solve the variational problem under the constraint that plastic deformation is irreversible. Numerical experiments are in agreement with classical solutions of slip-line field theory, but this model is much richer, since it allows to follow the nucleation and development of the slip bands as the boundary conditions are varied. By increasing the external load, new shear bands can be nucleated and/or the existing bands can become wider. Some bands may coalesce, whereas there may be zones only partially yielded, i.e., where the phase field takes an intermediate value between zero and one.

The yielding of thick long pipes under internal pressure has been examined in detail. The

elastic-plastic solution of our model is completely different from that obtainable from the classical continuum plasticity theory, since it implies a different location of the yielded zones in the form of slip bands crossing the entire thickness of the pipe, from the inner to the outer surface. This scenario is associated with a strain-softening internal-pressure vs. radial-displacement response, which can justify the unexpected brittle failures during the expansion stage that are often experienced in the UOE manufacturing process [36].

Of course, the theory is far from being exhaustive. A major limitation is in the fact that the material is considered perfectly plastic. This implies that the amount of slip on a band, as well as the work consumed on it, can be virtually infinite without producing material separation. Further developments may consists in introducing the possibility of work hardening, eventually followed by a strain-softening regime. In any case, it is remarkable, in our opinion, that in the proposed approach the *plastic* flow, traditionally described by macroscopic fields, is reconciliated with its origin, experimentally verified, from the relative slip of material portions along bands of very small thickness, with a kinematics somehow resembling that of a *fracture* opening under mode II. Moreover, the regularized approach is obtained through the introduction of the phase field, which is indeed analogous to a *damage* field, so that the model may be placed in the class of pseudo non-local gradient-damage models [40, 41, 42]. To this respect, a little step has perhaps being made towards the Aristotelian "*reductio ad unum*" principle for fracture, damage and plasticity, phenomena usually modelled with very different-in-type approaches, but that should be referable to one single entity within the broad science of the mechanics and physics of solids.

Acknowledgements. Support of the European Community European Community under grant RFCS-RFSR-CT-2012-00026 "S+G" is gratefully acknowledged.

[1] Hill R. The mathematical theory of plasticity. Oxford: Oxford University Press; 1998.

[2] Nadai A. Theory of flow and fracture of solids, Vol. 1. New York: McGraw-Hill Book Co.; 1950.

[3] Osakada K. History of plasticity and metal forming analysis. Journal of Materials Processing Technology 2010;210(11):1436–54.

[4] Del Piero G, Owen D. Structured deformations of continua. Archive for Rational Mechanics and Analysis 1993;124(2):99–155.

[5] Kirby S. Rock mechanics observations pertinent to the rheology of the continental lithosphere and the localization of strain along shear zones. Tectonophysics 1985;119(1-4):1–27.

[6] Yang B, Morrison M, Liaw P, Buchanan R, Wang G, Liu C, et al. Dynamic evolution of nanoscale shear bands in a bulk-metallic glass. Applied Physics Letters 2005;86(14):1–3.

[7] Ord A, Vardoulakis I, Kajewski R. Shear band formation in gosford sandstone. International Journal of Rock Mechanics and Mining Sciences 1991;28(5):397–409.

[8] Wolf H, Knig D, Triantafyllidis T. Experimental investigation of shear band patterns in granular material. Journal of Structural Geology 2003;25(8):1229–40.

[9] Bowden P, Jukes J. The plastic flow of isotropic polymers. Journal of Materials Science 1972;7(1):52–63.

[10] Cottrell AH. Dislocations and plastic flow in crystals. Oxford: Clarendon Press; 1965.

[11] Froli M, Royer-Carfagni G. A mechanical model for the elastic-plastic behavior of metallic bars. International Journal of Solids and Structures 2000;37(29):3901–18.

[12] Cox T, Low Jr. J. Investigation of the plastic fracture of aisi 4340 and 18 nickel - 200 grade maraging steels. Metallurgical Transactions 1974;5(6):1457–70.

[13] Tanaka K, Spretnak J. An analysis of plastic instability in pure shear in high strength aisi 4340 steel. Metallurgical Transactions 1973;4(2):443–54.

[14] Biolzi L, Royer-Carfagni G. Experimental evidence of serrated elastic-plastic deformation of metallic bars under torsion. In: Atti XV Congresso Nazionale AIMETA, Taormina, Italy. 2001, p. SPSO–04.

[15] Körber F, Siebel E. Zur theorie der bildsamen formänderung. Naturwissenschaften 1928;16(22):408–12.

[16] Rice J. The localization of plastic deformation. In: Koiter W, editor. Proceedings of the 14th International Congress on Theoretical and Applied Mechanics, Delft. Amsterdam: North-Holland; 1976, p. 207–20.

[17] Rittel D, Wang Z, Merzer M. Adiabatic shear failure and dynamic stored energy of cold work. Physical Review Letters 2006;96(7).

[18] Bigoni D. Nonlinear solid mechanics: bifurcation theory and material instability. Cambridge: Cambridge University Press; 2012.

[19] Bigoni D, Dal Corso F. The unrestrainable growth of a shear band in a prestressed material. Proceedings of the Royal Society A: Mathematical, Physical and Engineering Sciences 2008;464(2097):2365–90.

[20] Palmer AC, Rice J. The growth of slip surfaces in the progressive failure of over-consolidated clay. Proceedings of the Royal Society of London A: Mathematical, Physical and Engineering Sciences 1973;332(1591):527–48.

[21] Ambrosio L, Lemenant A, Royer-Carfagni G. A variational model for plastic slip and its regularization via -convergence. Journal of Elasticity 2013;110(2):201–35.

[22] Ambrosio L, Tortorelli VM. Approximation of functional depending on jumps by elliptic functional via t-convergence. Communications on Pure and Applied Mathematics 1990;43(8):999–1036.

[23] Hakim V, Karma A. Laws of crack motion and phase-field models of fracture. Journal of the Mechanics and Physics of Solids 2009;57(2):342–68.

[24] Del Piero G, Truskinovsky L. Elastic bars with cohesive energy. Continuum Mechanics and Thermodynamics 2009;21(2):141–71.

[25] Freddi F, Royer-Carfagni G. Plastic flow as an energy minimization problem. numerical experiments. Journal of Elasticity 2014;116(1):53–74.

[26] Ambrosio L, Fusco N, Pallara D. Special functions of bounded variations and free discontinuity problems. Oxford: Oxford University Press; 2000.

[27] Del Piero G. A variational approach to fracture and other inelastic phenomena. Journal of Elasticity 2013;112(1):3–77.

[28] Lancioni G, Royer-Carfagni G. The variational approach to fracture mechanics. a practical application to the french panthon in paris. Journal of Elasticity 2009;95(1-2):1–30.

[29] Bangerth W, Heister T, Heltai L, Kanschat G, Kronbichler M, Maier M, et al. The `deal.II` library, version 8.2. Archive of Numerical Software 2015;3.

[30] Heister T, Wheeler MF, Wick T. A primal-dual active set method and predictor-corrector mesh adaptivity for computing fracture propagation using a phase-field approach. Computer Methods in Applied Mechanics and Engineering 2015;290:466 –95.

[31] Burke S, Ortner C, Sli E. An adaptive finite element approximation of a generalized ambrosio-tortorelli functional. Mathematical Models and Methods in Applied Sciences 2013;23(9):1663–97.

[32] Negri M. Convergence analysis for a smeared crack approach in brittle fracture. Interfaces and Free Boundaries 2007;9(3):307–30.

[33] Freddi F, Royer-Carfagni G. Regularized variational theories of fracture: A unified approach. Journal of the Mechanics and Physics of Solids 2010;58(8):1154 –74.

[34] Hashford W, Caddell R. Metal Forming, Mechanics and Metallurgy. Cambridge University Press; 4th ed.; 2014.

[35] Chakrabarty J. Theory of Plasticity. Elsevier; 3th ed.; 2006.

[36] Herynk M, Kyriakides S, Onoufriou A, Yun H. Effects of the UOE/UOC pipe manufacturing processes on pipe collapse pressure. International Journal of Mechanical Sciences 2007;49(5):533–53.

[37] Zou T, Li D, Wu G, Peng Y. Yield strength development from high strength steel plate to UOE pipe. Materials and Design 2016;89:1107–22.

[38] Froli M, Royer-Carfagni G. Discontinuous deformation of tensile steel bars: Experimental results. Journal of Engineering Mechanics 1999;125(11):1243–50.

[39] Antaki GA. Piping and Pipeline Engineering: Design, Construction, Maintenance, Integrity, and Repair. New York: CRC Press; 2003.

[40] Frémond M, Nedjar B. Damage, gradient of damage and principle of virtual power. International Journal of Solids and Structures 1996;8:1083–103.

[41] Frémond M. Non-smooth thermomechanics. Heidelberg: Springer Verlag; 2001.

[42] Freddi F, Frémond M. Damage in domains and interfaces: a coupled predictive theory. Journal of Mechanics of Materials and Structures 2006;1:1205–34.